RSC Advances

ROYAL SOCIETY OF CHEMISTRY

www.rsc.org/advances

RSC advances

ARTICLE

Largely enhanced electrical properties of polymer composites via combined effect of volume exclusion and synergy

Received 00th January 20xx,
Accepted 00th January 20xx

DOI: 10.1039/x0xx00000x

www.rsc.org/

Kai Wu,[a] Linyu Wu,[a] Weixing Yang,[a] Songgang Chai,[b] Feng Chen*[a] and Qiang Fu*[a]

It has been demonstrated that introducing another non-conductive particles into conductive filler filled composites could result in a better conductivity due to volume exclusion effect. It was also reported that combining electrically conductive fillers with different geometric shapes and aspect ratio together could enhance the electrical conductivity as due to the synergistic effect. To further explore these two effects on the electrical property enhancement, we firstly encapsulated neat silica (SiO_2) with graphene oxide (GO) through electrostatic self-assembly to render SiO_2 with surface conductivity. Then neat SiO_2 or SiO_2@GO together with multi-walled carbon nanotubes (MWCNT) were mixed with polystyrene (PS) to prepare conductive composites. In this way, volume exclusion effect in PS/MWCNT/SiO_2 system and combined effect of volume exclusion and synergy in PS/MWCNT/SiO_2@rGO system could be investigated and compared. An obvious increased conductivity was observed only in the transition composition region for PS/MWCNT/SiO_2 system compared with PS/MWCNT system. However, a largely enhanced conductivity was achieved in all the composition region for PS/MWCNT/SiO_2@rGO system compared with PS/MWCNT/SiO_2 system and PS/MWCNT, companied with greatly enhancement of Electromagnetic Interference (EMI) shielding effectiveness. Concluded from SEM characterization and rheological properties, we attributed this obvious enhanced electrical property to both volume exclusion effect and synergistic effect.

1. Introduction

Conductive polymer composites (CPCs) have attracted comprehensive interest owing to their various applications, such as strain and damage sensing, stretchable conductor, thermoelectric materials and electromagnetic shielding.[1-13] CPCs are usually fabricated through incorporating single or hybrid conductive fillers (e.g. carbonaceous, conductive polymeric particles and metallic) with polymer matrix. As increase of filler concentration, the CPCs will exhibit an insulator/conductor transition, with a jump in electrical conductivity by several orders of magnitude. This phenomenon is defined as electrical percolation, and the critical fraction is termed the percolation threshold. A lot of work has been done to reduce the percolation threshold. For instance, designing polymer blends to selectively locate conductive fillers in one of the polymer phases or at the interfaces[14, 15]; using thermal annealing above the glass transition temperature or melting temperature of polymer to induce the formation of conductive network[16, 17]; using shear force to trigger orientation of conductive fillers[18, 19]; using polymer latex particles to form segregated network[20, 21]; using electric or magnetic field to control the morphology of conductive network[22, 23]; preforming highly porous and compact 3-D conductive framework in polymer matrix[10].

Among these methods, volume exclusion effect via introducing another non-conductive particles, such as clay, silica and calcium carbonate, to form a segregated conductive structure is considered to be significant to decrease the percolation threshold.[24-26] This is ascribed to the fact that the conductive fillers tend to be excluded from non-conductive particles dominated areas, leading to higher effective concentration of conductive fillers.[25] However, the idea of volume exclusion does not always work, it depends on the size and volume content of non-conductive particles, the interaction between conductive and non-conductive particles, as well as the combination of conductive and non-conductive particles. For example, at the regions below or above percolation threshold, addition of non-conductive particles only results in a limited increase of conductivity, while a largely enhanced conductivity is observed at the vicinity of transition. On the other hand, it was also reported that mixing electrically conductive fillers with different geometric shapes and aspect ratio in polymer matrix may show synergistic effect that will increase the electrical conductivity of the composites.[27-31] So far, the effect of volume exclusion and synergistic on the electrical conductivity of polymer composites has been investigated separately. If the non-conductive particles are coated with a thin layer of conductive material, one expects a combined effect of volume exclusion and synergy. How does the conductivity of CPCs change if adding surface coated non-conductive particles? Will it be extend to

[a] College of Polymer Science and Engineering, State Key Laboratory of Polymer Materials Engineering, Sichuan University, Chengdu 610065, China. Tel: +86-28-85460690 (F.C.). Tel/Fax: +86-28-85461795 (Q.F.). E-mail: fengchen@scu.edu.cn (F.C.); qiangfu@scu.edu.cn (Q.F.).

[b] Guangdong Shengyi Technology Limited Corporation, Dongguan, 523039, China.

all the composition region for the enhancement of conductivity? These questions would be very interesting and worth to be explored.

For this reason, in this study, we firstly studied the volume exclusion effect of 20 wt% neat silica (SiO_2) particles through incorporating them with muti-walled nanotubes (MWCNT) using PS as polymer matrix. Only at the percolation threshold, the electrical conductivity did exhibit increase with orders of magnitude. At other concentrations, a limited enhancement in electrical conductivity was obtained in comparison with that of PS/MWCNT, which was similar to the results in the previous study.[25] Hence increasing the loading of electrically inert SiO_2 was necessary for effectively enhance the electrical property according to previous report. In order to avoid introducing a mass of non-conductive particles in sacrifice of mechanical property and processability, core-shell structure of modified SiO_2 was prepared which can render SiO_2 with surface conductivity. To do this, the surface of SiO_2 was wrapped with graphene oxide (GO) thin layer through mutual electrostatic interactions in the aqueous solution. The surface coated SiO_2 was added again in to PS/MWCNT composites to investigate the combined effect of volume exclusion and synergy, since the GO layer could be thermally reduced via compression molding at high temperature. The effect of thermal reduction on GO was confirmed by TGA, FTIR and Raman spectra. As consequences, a largely enhanced conductivity was achieved in all the composition region for PS/MWCNT/SiO_2@rGO system compared with PS/MWCNT/SiO_2 system and PS/MWCNT, companied with greatly enhancement of Electromagnetic Interference (EMI) shielding effectiveness. SEM characterization and rheological test were carried out to understand the mechanism of property enhancement.

2. Experimental

2.1 Materials

Graphite powders were purchased from Qingdao Black Dragon graphite Co., Ltd. Micron sized silica (average diameter: 5 μm) and 3-aminopropyltriethoxysilane (APS) were purchased from Aladdin Chemicals Co., Ltd. Potassium permanganate ($KMnO_4$), sulfuric acid (H_2SO_4 98%), hydrogen peroxide (H_2O_2), hydrochloric acid, ethanol and N,N-dimethylformamide (DMF) were supplied by Kelong Chemical reagent plant (Chengdu, China). Multi-walled carbon nanotubes (MWCNT, NC7000, 1.5um in length, diameter of 9.5nm) were purchased from Nanocyl S.A., Belgium. Amorphous polystyrene (PS, PG33, 1.04 g/cm^3) was purchased from Sino-foreign Joint Venture Zhenjiang Qimei Chemical Co., Ltd.

2.2 Surface modification of SiO_2 by APS and encapsulation by GO

Similar to previous studies,[32] the core-shell structure of SiO_2@GO hybrid was fabricated by two environmental steps: the surface modification of SiO_2 particles with APS and the electrostatic self-assembly between GO and the modified SiO_2.

GO was prepared through the exfoliation of natural graphite by Hummers method.[33] Then the exfoliated GO was collected by centrifugation to remove the nonexfoliated graphite. After that, steady GO aqueous solution was achieved by sonication in deionized water for 2 h.

The modification of SiO_2 was prepared according to our previous study.[34] In a typical process, according to **Figure 1 (1)**, SiO_2 particles (10 g) were dispersed well in 300 ml ethanol solution (ethanol: H_2O=95:5), being mixed with 0.5 ml of silane coupling agent APS. Then, the solution was kept at 60℃ overnight for reaction. After that, the obtained product SiO_2-NH_2 was washed by deionized water and ethanol for 2 times, and dried under vacuum.

The electrostatic self-assembly between GO and the SiO_2-NH_2 was achieved through a simple procedure, as is shown in **Figure 1 (2)**. 1000 ml GO aqueous solution (0.15 mg/ml) and 500 ml SiO_2-NH_2 suspension (20 mg/ml) were mixed together under mild magnetic stirring for 2 h. Then, the SiO_2@GO powder with the GO concentration of 1.5 wt% was collected by centrifugation and dried under vacuum.

2.3 Preparation of PS-based composites

For the fabrication of PS/MWCNT/SiO2@rGO, according to **Figure 1 (3)**, the desired amount of fillers were dispersed well in DMF through mild magnetic stirring and sonication. Meanwhile, 10 g PS was dissolved in 50 ml DMF at 60 ℃. Afterwards, the fillers suspension was mixed with PS solution well through intense mechanical stirring and then both fillers and PS were precipitated in deionized water. The collected precipitation was dried under vacuum and then processed into specimens by compression molding at 200℃ for 40min, simultaneously thermally reducing GO to rGO. PS, PS/MWCNT, PS/MWCNT/SiO_2 nanocomposites were prepared in a similar solution.

2.4 Characterization

Scanning electron microscopy (SEM) images of silica were obtained by using the scanning electron microscopy (SEM, Inspect F, FEI Company, USA). The cryo-fractured surfaces of PS/MWCNT/SiO_2 and PS/MWCNT/SiO_2@rGO nanocomposites were characterized to observe the morphology. The fractured surfaces were prepared in liquid N_2 and were sputtered with gold in vacuum prior to observation.

Energy dispersive X-ray spectrometry (EDS) was utilized to analyze the composition of elements in GO, SiO_2, SiO_2-NH_2, SiO_2@GO to prove the encapsulation of GO on the surface of SiO_2 particles.

Zeta potential measurements were characterized using a Zetasizer 3000 (Malvern Instruments). Before measurement, GO and silica aqueous solution were respectively diluted to 0.05, 2 mg/ml.

Raman spectra of GO and SiO_2@GO were characterized with a laser wavelength of 532 nm.

Fourier Transform Infrared (FTIR, Nicolet 6700) spectroscopy was carried out to characterize the functional groups in GO and rGO to discuss the influence of thermal reduction on GO.

The thermal stability and thermal reduction influence was studied with Thermal Gravimetric Analysis (TGA, TA instrument, Q500, USA). The temperature increased from 30 to 600℃ for composites and 30 to 760℃ for GO at a heating rate of 10℃/min in nitrogen atmosphere.

The electrical conductivity of the samples was characterized with a Keithley 6487 picoammeter under a constant voltage of 1 V in order to avoid strong electric current within the specimen. To prevent

contact resistance, silver paint was brushed on the both ends of the samples.

Melt rheology of PS, PS/MWCNT/SiO_2 and PS/MWCNT/SiO_2@rGO nanocomposites was measured in a strain-controlled dynamic rheometer Bohlin Gemini 200, Malvern Instruments, British. In order to achieve a linear viscoelastic response, the frequency sweep was set in the range of 0.01-100 Hz with the strain amplitude of 1%. Disk-shaped samples from compression molding with the diameter of 25 mm and thickness of 18 mm were used during this characterization.

EMI shielding characteristics of the samples with the diameter of 13 mm and thickness of 1.3 mm report here were measured by us using a coaxial test cell (APC-7 connector) connected with an Agilent N5230 vector network analyzer.

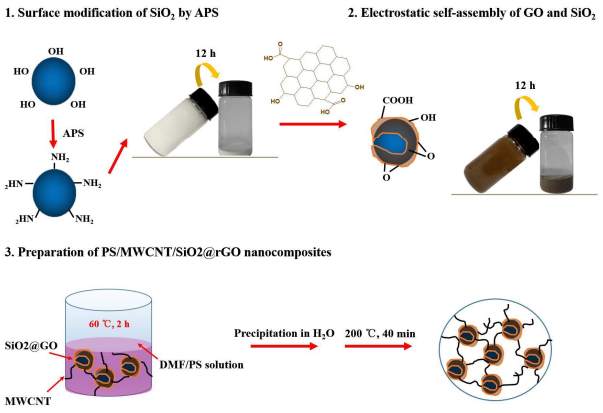

Figure 1. Preparation steps of PS/MWCNT/SiO_2@rGO nanocomposites shown in this scheme. (1) SiO_2 is modified by APS; and images of SiO_2-NH_2 solution before and after 12 h. (2) GO encapsulates SiO_2-NH_2 by electrostatic attraction; and images of SiO_2@GO solution before and after 12 h. (3) The method of mixing PS, MWCNT and SiO_2@GO; and the schematic of dispersion of fillers in the PS matrix.

3. Results and discussion

3.1 Electrostatic assembly of GO and APS-modified SiO_2

Two-dimensional GO nanosheets ionized negative charge in aqueous solution owing to large amount of carboxylic acid group on their surface. Driven by the mutual electrostatic interactions, the sheets can encapsulate many positively charged particles when mixed them in aqueous solution together.[32, 35, 36] In this study, in order to make SiO_2 particles carry groups which can ionized positive charge in aqueous solution, they were modified by APS. As a result, amino groups (-NH_2) were grafted onto the surface of SiO_2 particles. In aqueous solution with the pH value of 7.0, the surface charge of GO, SiO_2 and SiO_2-NH_2 was respectively characterized by zeta potential tests. GO and unmodified SiO_2 both had highly negative surface charge with ξ potential value of -57.80 mV and -42.16 mV. After modification, the surface charge of SiO_2-NH_2 was positive (ξ potential = +52.13 mV). It suggested that successful graft of APS onto the surface of SiO_2 was achieved. Then, the positively charged SiO_2-NH_2 and negatively charged GO were mixed together and they assembled into a whole. To confirm the truth of the core-shell structure of SiO_2@GO, the morphology and constituent elements were characterized, and the results are shown in the **Figure 2**.

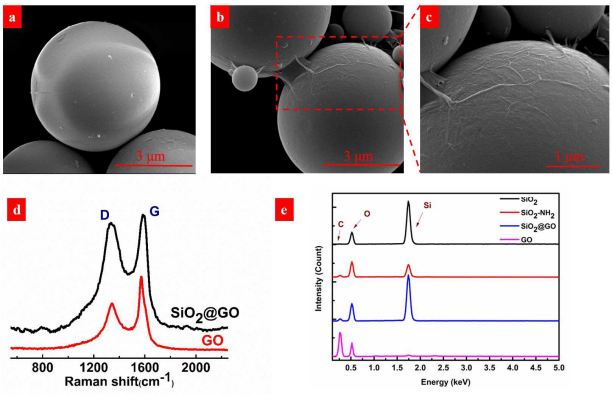

f

Samples	Relative atomic percentage (%)		
	C	O	Si
SiO2	6.73	56.26	37.01
SiO_2-NH2	12.32	54.60	33.09
SiO_2@GO	21.55	53.69	24.76
GO	54.54	45.46	0

Figure 2. Typical SEM images of (a) SiO_2 and (b, c) SiO_2@GO; (d) Raman spectra of GO and SiO_2@GO; (e, f) EDX analysis of SiO_2, SiO_2-NH_2, SiO_2@GO and GO.

According to **Figure 2 (a)**, the surfaces of micron SiO_2 particles are smooth. After modified by APS and encapsulated by GO sheets, one can clearly observe that there are some ultrathin GO sheets and folds firmly fixed on the surface of SiO_2, as is shown in the **Figure 2 (b) and (c)**. Raman spectroscopy is considered as a powerful tool to capture the presence of graphene and its derivatives. According to the **Figure 2 (d)**, by means of Raman spectroscopy, the D and G band similar to these of original GO are observed at 1337 cm^{-1} and 1589 cm^{-1}. It is known that GO disperses well in aqueous solution, even though exposed to the centrifugal environment of 5000 rpm/min. So the existence of the characteristic peaks of GO indicates that the GO was not removed by centrifugation but attracted by SiO_2-NH_2 to form the core-shell structure. And it is interesting to find that the intensities of both the bands increases compared to these of GO under the same conditions characterized. We consider that the presence of GO on the surface of SiO_2 results in the surface enhanced Raman effect (SERS), but the mechanism is still under study and the preliminary explanation is given as follows. Because GO absorbed on SiO_2 could use the attached functional groups as nucleation centers.[37, 38] Based on the chemical mechanism of SERS, such electrostatic interaction could generate the charge-transfer complex to absorb light at the excitation frequency, resulting in chemical SERS. To further confirm the encapsulation of SiO_2 particles by GO sheets and the effective grafting of APS, elemental analysis was also applied. As is shown in the **Figure 2 (e)** and **(f)**, the relative atomic percentages of C, O and Si are respectively 6.73, 56.26 and 37.01. After being modified by APS, the relative atomic percentage of C obviously increases but the relative atomic percentages of O and Si decrease. Because for APS, the relative

atomic percentages of Si and O are less than those of SiO_2, but the relative atomic percentage of C is more than that of SiO_2. So it suggests that APS was successfully grafted to SiO_2. For SiO_2@GO, the rise of C content from 12.32% of SiO_2-NH_2 to 21.55% also indicates the immobilization of GO on the SiO_2.

3.2 The reduction of GO

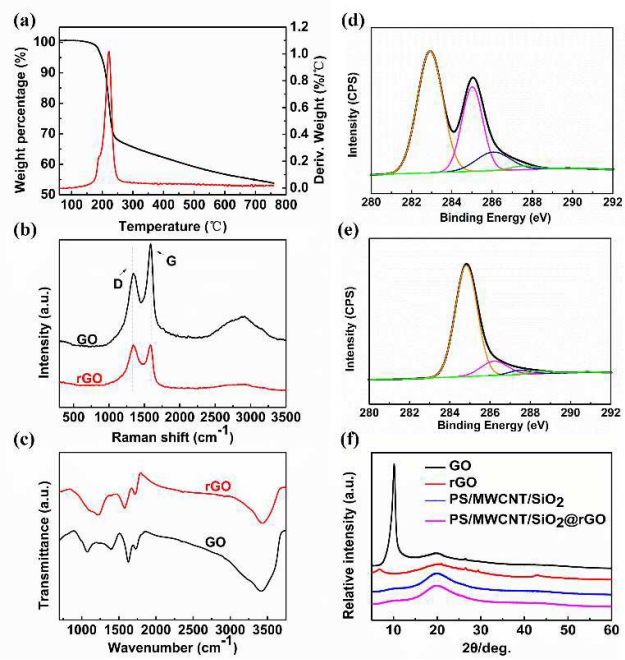

Figure 3. (a) TGA test of GO as function of temperature from 60℃ to 760℃ (Weight percentage/ blue line; Deriv. Weight/red line); (b) FTIR spectra of GO and thermally reduced rGO; (c) Raman spectra of GO and rGO via thermal reduction. XPS C_{1s} core-level spectra of (d) GO and (e) rGO. The main peaks observed in both the pictures respectively correspond to sp^2 C (orange), sp^3 C (purple), C-O (blue) and C=O (green); (f) XRD patterns of GO, rGO, PS/MWCNT/SiO_2 and PS/MWCNT/SiO_2@rGO. The concentrations of MWCNT and modified SiO_2 are 2 wt% and 20 wt%, respectively.

In order to determine the temperature for reducing GO, we firstly carried out the TGA experiment, as is shown in the **Figure 3 (a)**. From the TGA results, it is observed that GO exhibits fast weight loss at about 170~250 ℃, suggesting that abundant oxygen-containing functional groups can be removed above 170℃. Hence, we prepared the PS nanocomposites above this temperature for 40 min to mildly reduce GO. FTIR spectra was utilized to discuss the degree of reduction from GO to rGO, and the results are shown in the **Figure 3 (b)**. One can find that GO exhibits these characteristic peaks: C=O (1730 cm^{-1}), O-H (1622 cm^{-1}), carboxyl C-O (1414 cm^{-1}), epoxy C-O (1228 cm^{-1}).[39-41] After mild thermal reduction, it is obvious that the characteristic peaks for oxygen functional groups decrease. Especially, carboxyl C-O at 1414 cm^{-1} has disappeared. And the original aromatic C=C peak at 1622 cm^{-1} shifts to 1577 cm^{-1}, which is similar to the previous report.[40] Furthermore, Raman spectra results plotted in the **Figure 3 (c)** show that the intensity ratio of the D and G band (I_D/I_G) changes from 0.684 to 0.974, suggesting the increase in average size of sp^2 domain after thermal reduction.[40] Similar phenomenon was observed by Paredes et al.[42], Kaner et al.[43] and Stankovich et al.[44] through chemical reduction. It was reported that reduction would cause the more aromatic domains of small overall size in rGO, leading to enhanced I_D/I_G ratio.[44] Besides, the G band for rGO is shifted from 1589 cm^{-1} to 1586 cm^{-1}, which is closer to that of pristine graphite, demonstrating the successfully reduction through this procedure. Moreover, XPS was also utilized to characterize the reduction of GO. According to XPS results, the C and O atomic percentage content were respectively 76.48 % and 23.52 %. The relatively high O content is ascribed to the rich oxygen-containing functional groups, according to the **Figure 3 (d)**. After reduction, one can find that the oxygen peaks were obviously weakened (**Figure 3 (e)**), with the C and O atomic percentage content of 91.07 % and 8.93 %, indicating successfully reduction of GO. XRD is also an important tool to characterize the GO derivatives and its nanocomposites.[45, 46] Observed from the **Figure 3 (f)**, the typical diffraction peak of GO was at 10.2°, corresponding to a certain interlayer spacing. After being reduced, this characteristic peak almost disappeared, indicating most of oxygen-containing functional groups were reduced. Moreover, no such peak was seen in PS/MWCNT/SiO_2@rGO nanocomposites, which suggests that the periodic structure of GO disappeared and the sheets were exfoliated owing to absorption and uniform dispersion of SiO_2@rGO.

3.3 Electrical property of PS nanocomposites

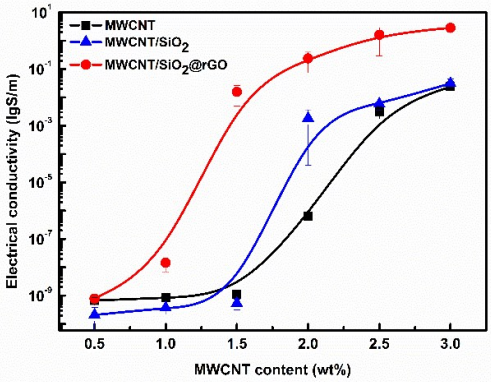

Figure 4. The electrical conductivity of PS/MWCNT, PS/MWCNT/SiO_2 and PS/MWCNT/SiO_2@rGO nanocomposites as increase of MWCNT. (The mass fractions of SiO_2 and SiO_2@rGO are all fixed at 20 %.)

PS/MWCNT nanocomposites have good electrical properties owing to excellent electrically conductive feature of MWCNT.[47-51] It is well-known that introducing non-conductive particles into conductive fillers filled polymer may result in enhanced electrical conductivity due to volume exclusion effect. Moreover, mixing electrically conductive fillers with different geometric shapes and aspect ratio together in polymer matrix may lead to synergistic effect that will enhance the electrical conductivity of the complex. So we respectively combined SiO_2 and this hybrid filler with PS and MWCNT. In order to study the difference of electrical conductivity between respectively introducing SiO_2 and SiO_2@rGO to

PS/MWCNT, the DC electrical conductivity of the three types of PS nanocomposites is discussed as follows. According to the **Figure 4**, the electrical conductivity of all the three types of PS nanocomposites increases as increase of MWCNT content. Before the percolation threshold, the upward trend of the electrical conductivity is not obvious. At the percolation threshold, a sharp increase of the electrical conductivity is observed according to the three curves, indicating an insulator-conductor transition at this time. After the percolation threshold, the upward trend tends to be gentle. Besides, one can find that the electrical conductivity of PS/MWCNT/SiO_2 is relatively higher than that of PS/MWCNT especially near the percolation threshold. At the concentration of 2 wt%, increment in electrical conductivity with three orders of magnitude compared to that of PS/MWCNT can be observed. But at other concentrations, the enhancement is not obvious, suggesting that volume exclusion effect is not always work when the loading of non-conductive filler is not high enough. However, for PS/MWCNT/SiO_2@rGO, the electrical conductivity is always much higher than that of PS/MWCNT/SiO_2 or PS/MWCNT at the same content of MWCNT, particularly at the percolation threshold of MWCNT. One can observe that, at the MWCNT loading of 1.5 wt%, much higher electrical conductivity for PS/MWCNT/SiO_2@rGO is obtained, presenting a jump with eight orders of magnitude compared to that of PS/MWCNT/SiO_2 and PS/MWCNT. It suggests that the percolation threshold of PS/MWCNT/SiO_2@rGO is largely reduced owing to the role of extremely few rGO coated on the surface of SiO_2, and the mechanism will be discussed below.

3.4 Mechanism for enhanced electrical conductivity

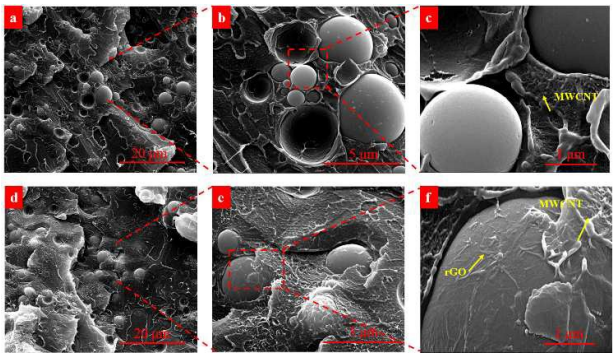

Figure 5. Scanning electron microscopy micrographs from hybrid PS nanocomposites specimens with (a), (b) and (c) 20 wt% SiO_2 and 2 wt% MWCNT; (d), (e) and (f) 20 wt% SiO_2@rGO and 2 wt% MWCNT. The magnification from (a) to (c) and (d) to (f) is higher and higher.

In order to truly observe the morphology and dispersed state of fillers to propose the mechanism, the cryo-fractured surfaces of PS/MWCNT/SiO_2 and PS/MWCNT/SiO_2@rGO nanocomposites were characterized by SEM, as is shown in the **Figure 5**. According to the **Figure 5 (a)** and **(b)**, one can observe that unmodified SiO_2 particles whose surface is smooth disperse relatively homogeneous in PS matrix. And these large SiO_2 particles can exclude MWCNT from their dominant areas, so MWCNT can connect with each other in a higher probability. As consequence, the effective concentration of MWCNT is increased (see the **Figure 5 (c)**). For PS/MWCNT/SiO_2@rGO, the dispersed state of both MWCNT and SiO_2@rGO is similar to that of PS/MWCNT/SiO_2. Because PS/MWCNT/SiO_2 and PS/MWCNT/SiO_2@GO nanocomposites were prepared in the DMF solution via intense mechanical stirring. When they were precipitated in deionized water, the dispersed state of SiO_2 and SiO_2@GO in PS matrix was fixed. Hence, when these nanocomposites were compressed and reduced at high temperature, the filler dispersion of SiO_2 and SiO_2@rGO in PS matrix was similar although the interaction between rGO and PS is good. However, from the **Figure 5 (e)** and **(f)**, one can find that the conductive rGO folds fixed firmly on the surface of SiO_2 are connected well with MWCNT as due to π-π interactions, and this conductive rGO shell make non-conductive SiO_2 become conductive particles through transforming electrons by surficial immobilized rGO. So we deem that this would result in not only increased effective concentration of MWCNT owing to volume exclusion effect of SiO_2@rGO, but also improved conductive network owing to synergistic effect.

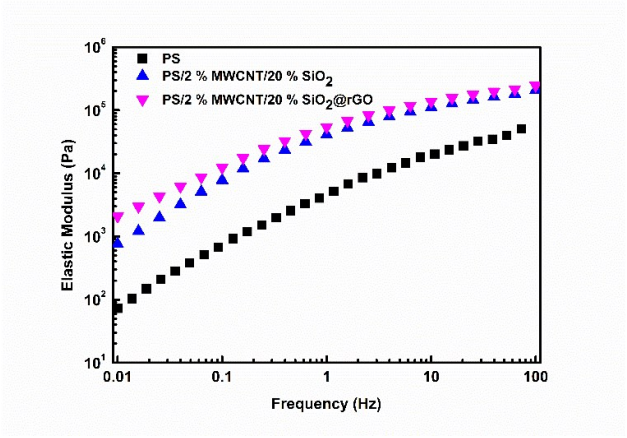

Figure 6. Elastic modulus (G') of PS and PS composites as function of frequency.

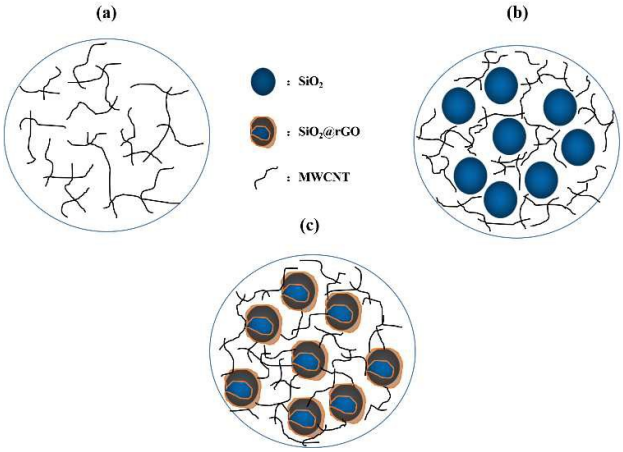

Figure 7. Schematic of fillers' dispersed state in PS nanocomposites: (a) PS/MWCNT; (b) PS/MWCNT /SiO_2; (c)PS/MWCNT/SiO_2@rGO.

Rheological properties of molten composites are considered to be effective to reflect the filler dispersion state. Since SEM

observation demonstrated that the dispersed state of the fillers for both PS/MWCNT/SiO_2 and PS/MWCNT/SiO_2@rGO are similar, in order to prove this observation further, the melt rheology of PS nanocomposites was measured and the results were plotted in the **Figure 6**. In melt rheology test, PS nanocomposites filled with 2 wt% MWCNT were randomly selected as the example. Clearly the composites Modulus are higher than that of neat PS. Specifically, PS/2 % MWCNT/SiO_2@rGO exhibits comparative elastic modulus in comparison with that of PS/2 % MWCNT/SiO_2, indicating that unchanged dispersed state of SiO_2 and MWCNT in PS matrix after encapsulation by rGO. So the largely enhanced electrical conductivity and obviously decreased percolation threshold are ascribed to both volume exclusion and synergistic effects discussed below instead of improved dispersion for fillers.

To vividly explain the mechanism concluded from the discussions above, a schematic of fillers' dispersed state in PS nanocomposites is plotted in the **Figure 7**. For MWCNT uniformly dispersing in PS, conductive network needs a certain amount of fillers which are so close that can meet with electron transition. Hence the electrons can pass through the composites by the MWCNT network. Once vast non-conductive SiO_2 particles are added, these large-size granules will exclude MWCNT from their dominant regions, leading to increased effective concentration of MWCNT that form conductive network in the segregated areas. According to the previous report[25], the effective concentration of MWCNT is defined as $V_{MWCNT}/(V_{MWCNT}+V_{polymer})$. Hence, for example, when only 20 wt% SiO_2 was added, the effective concentration of MWCNT increased by 9.5% at the MWCNT loading of 1.5 wt%, resulting in enhancement with orders of magnitude in electrical conductivity near the percolation threshold. However, after the percolation, the increased effective concentration is limited, thus leading to inconspicuous enhancement in electrical properties compared to that of PS/MWCNT. But for PS/MWCNT/SiO_2@rGO, although encapsulation by rGO has not changed the dispersion trait entirely, SiO_2@rGO can be considered as electrically conductive particles which conduct electrons through rGO on the surface of insulating SiO_2. Moreover, different from poor interactions and separation between unmodified SiO_2 and MWCNT, the rGO coated on the surface of particles make them connect well with MWCNT due to π-π interactions. As a result, not only do these SiO_2@rGO isolate MWCNT from their occupied space on account of volume exclusion effect, but also link the gaps present between the unconnected MWCNT to perfect the conductive network. This is mainly ascribed to different geometric shapes and aspect ratio as well as dispersion features between SiO_2@rGO and MWCNT. Hence, the electrical conductivity of PS/MWCNT/SiO_2@rGO demonstrated a largely enhanced result.

3.5 Electromagnetic Interference (EMI) shielding effectiveness

Owing to the obvious increase in electrical conductivity of PS/MWCNT/SiO_2@rGO nanocomposites, this prepared material is considered to possess potential application in EMI shielding.[10, 52] For this reason, the EMI shielding effectiveness (SE) was studied and this was plotted in the **Figure 8**. One can see that for all the three types of PS nanocomposites, the EMI shielding effectiveness increases as increase of MWCNT content. The shielding effectiveness of PS/MWCNT/SiO_2 with 2 wt% MWCNT loading shows shielding effectiveness of 13.2-21.9 dB over the frequency of 8-12 GHz. Further raising MWCNT content to 3 wt%, the SE of PS/MWCNT/SiO_2 increases to 13.8-27.1 dB, which is quite with that of PS/MWCNT because of comparative electrical conductivity. Furthermore, one can find that the EMI shielding effectiveness of PS/MWCNT or PS/MWCNT/SiO_2 is sensitive to frequency. However, for PS/MWCNT/SiO_2@rGO, the shielding effectiveness is almost independent of frequency in the measured frequency region. And the shielding effectiveness is relatively higher at the same frequency, especially at the low frequency. For example, at the MWCNT content of 3 wt%, the EMI shielding effectiveness of PS/MWCNT/SiO_2@rGO increased 16.5 dB (almost 120%) at 8 GHz compared to that of PS/MWCNT/SiO_2. This largely improved EMI property is mostly ascribed to more complete conductive network and higher electrical conductivity of PS/MWCNT/SiO_2@rGO. According to previous study, this high electrical conductivity and good EMI properties are comparative with those of PS/graphene composites at the same filler concentration.[53-56] However, why the frequency-dependence for PS/MWCNT/SiO_2@rGO is different from that of PS/MWCNT or PS/MWCNT/SiO_2 is not understood and this will be studied in the future.

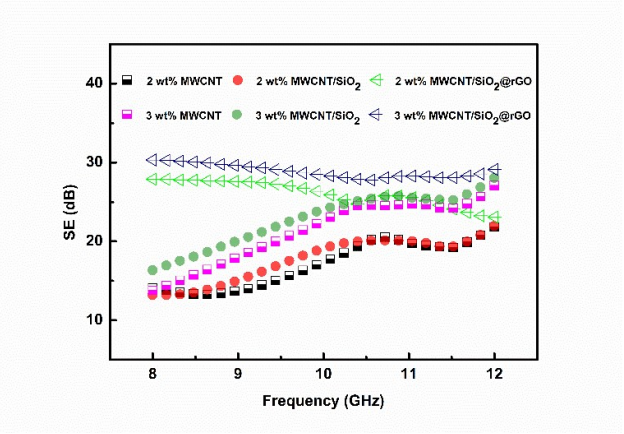

Figure 8. Electromagnetic Interference shielding effectiveness of PS/MWCNT, PS/MWCNT/SiO_2 and PS/MWCNT/SiO_2@rGO nanocomposites as a function of frequency measured in 8-12 GHz range.

3.6 Thermal stability

Thermal stability is important for PS composites no matter in melt processing or high temperature application. Hence, TGA study was used to investigate the effects of different fillers on the thermal stability of PS nanocomposites, and the results were plotted in the **Figure 9**. Except for the adsorbed water, there is almost no mass loss at the temperature lower than 350℃. According to the **Figure 9 (a)**, one can judge that the SiO_2 or SiO_2@rGO loading is 20 wt%, and the content of rGO is scarcely (≤0.2 wt%). Obtained from the **Figure 9 (b)**, PS/MWCNT decomposes rapidly at 415.8℃, and the presence of 20 wt% SiO_2 in the PS/MWCNT nanocomposites reduce the thermal stability, leading to the reduction of the maximum decomposition temperature (414.6 ℃). After the SiO_2 being encapsulated by rGO, the maximum decomposition temperature

increases to 416.2 ℃. However, the difference is not great. It suggests that either adding SiO_2 or introducing SiO_2@rGO to PS/MWCNT, the thermal stability of PS nanocomposites are well maintained.

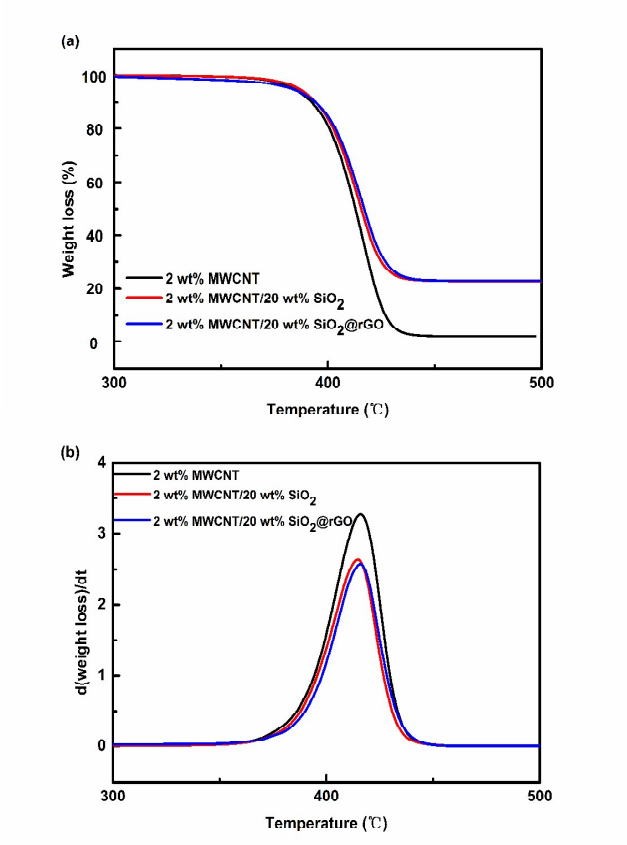

Figure 9. (a) Thermal Gravimetric Analysis test and (b) derivative of weight change curve of PS/MWCNT, PS/MWCNT/SiO_2 and PS/MWCNT/SiO_2@rGO nanocomposites. The MWCNT content of all the specimens are fixed as 2 wt%.

4. Conclusion

The core-shell structure of SiO_2@GO has been successfully prepared by a simple solution blending method. And the application of this hybrid filler in PS/MWCNT demonstrates the enhanced electrical conductivity and EMI shielding effectiveness. We attribute the enhancement to the volume exclusion effect of SiO2@rGO as well as synergistic effect between SiO2@rGO and MWCNT. And we believe that our study will provide a better understanding of volume exclusion effect and synergistic effect for the enhancement of electrical property.

Acknowledgement

This work was supported by the National Natural Science Foundation of China (51421061 and 51210005). We would like to express our great thanks to Guangdong Shengyi Technology Limited Corporation for financial support.

Notes and references

1. H. Deng, T. Skipa, E. Bilotti, R. Zhang, D. Lellinger, L. Mezzo, et al., *Advanced Functional Materials*, 2010, **20**, 1424-32.
2. H. Deng, L. Lin, M. Ji, S. Zhang, M. Yang, Q. Fu, *Progress in Polymer Science*, 2014, **39**, 627-55.
3. S. Maiti, N. K. Shrivastava, S. Suin, B. B. Khatua, *ACS Appl Mater Interfaces*, 2013, **5**, 4712-24.
4. V. Eswaraiah, K. Balasubramaniam, S. Ramaprabhu, *Journal of Materials Chemistry*, 2011, **21**, 12626-8.
5. T. Sekitani, Y. Noguchi, K. Hata, T. Fukushima, T. Aida, T. Someya, *Science*, 2008, **321**, 1468-72.
6. C. A. Hewitt, A. B. Kaiser, S. Roth, M. Craps, R. Czerw, D. L. Carroll, *Nano letters*, 2012, **12**, 1307-10.
7. M. H. Al-Saleh, U. Sundararaj, *Carbon*, 2009, **47**, 1738-46.
8. S. P. Pawar, K. Pattabhi, S. Bose, *RSC Advances*, 2014, **4**, 18842-52.
9. Y. Chen, Y. Li, D. Xu, W. Zhai, *RSC Advances*, 2015, **5**, 82034-41.
10. Y. Chen, H. B. Zhang, Y. Yang, M. Wang, A. Cao, Z. Z. Yu, *Advanced Functional Materials*, 2016, **26**, 447-55.
11. Y. Chen, Y. Wang, H.-B. Zhang, X. Li, C.-X. Gui, Z.-Z. Yu, *Carbon*, 2015, **82**, 67-76.
12. Y. Chen, H.-B. Zhang, Y. Huang, Y. Jiang, W.-G. Zheng, Z.-Z. Yu, *Composites Science and Technology*, 2015, **118**, 178-85.
13. H.-B. Zhang, Q. Yan, W.-G. Zheng, Z. He, Z.-Z. Yu, *ACS applied materials & interfaces*, 2011, **3**, 918-24.
14. A.-C. Baudouin, J. Devaux, C. Bailly, *Polymer*, 2010, **51**, 1341-54.
15. A. Göldel, G. Kasaliwal, P. Pötschke, *Macromolecular rapid communications*, 2009, **30**, 423-9.
16. C. Zhang, L. Wang, J. Wang, C.-a. Ma, *Carbon*, 2008, **46**, 2053-8.
17. I. Alig, P. Pötschke, D. Lellinger, T. Skipa, S. Pegel, G. R. Kasaliwal, et al., *Polymer*, 2012, **53**, 4-28.
18. D. Lellinger, D. Xu, A. Ohneiser, T. Skipa, I. Alig, *physica status solidi (b)*, 2008, **245**, 2268-71.
19. E. N. J. Ford, M. L. Minusa, T. Liu, J. I. Choi, S. S. Jang, S. Kumar, *Macromolecular Chemistry and Physics*, 2012, **213**, 617-26.
20. S. M. Miriyala, Y. S. Kim, L. Liu, J. C. Grunlan, *Macromolecular Chemistry and Physics*, 2008, **209**, 2399-409.
21. I. Jurewicz, P. Worajittiphon, A. A. King, P. J. Sellin, J. L. Keddie, A. B. Dalton, *The Journal of Physical Chemistry B*, 2011, **115**, 6395-400.
22. B. W. Steinert, D. R. Dean, *Polymer*, 2009, **50**, 898-904.
23. H. Pang, C. Chen, Y.-C. Zhang, P.-G. Ren, D.-X. Yan, Z.-M. Li, *Carbon*, 2011, **49**, 1980-8.
24. M. Kotaki, K. Wang, M. L. Toh, L. Chen, S. Y. Wong, C. He, *Macromolecules*, 2006, **39**, 908-11.
25. H.-D. Bao, Z.-X. Guo, J. Yu, *Polymer*, 2008, **49**, 3826-31.
26. W. Zhang, R. S. Blackburn, A. A. Dehghani-Sanij, *Scripta materialia*, 2007, **56**, 581-4.
27. S. Zhang, L. Lin, H. Deng, X. Gao, E. Bilotti, T. Peijs, et al., *Express Polym Lett*, 2012, **6**, 159-68.
28. M. Safdari, M. S. Al-Haik, *Carbon*, 2013, **64**, 111-21.
29. K.-S. Kim, S.-J. Park, *Carbon letters*, 2012, **13**, 51-5.

30. Z.-Y. Xiong, B.-Y. Zhang, L. Wang, J. Yu, Z.-X. Guo, *Carbon*, 2014, **70**, 233-40.
31. M.-C. Hermant, P. van der Schoot, B. Klumperman, C. E. Koning, *Acs nano*, 2010, **4**, 2242-8.
32. S. Yang, X. Feng, S. Ivanovici, K. Müllen, *Angewandte Chemie International Edition*, 2010, **49**, 8408-11.
33. W. S. Hummers Jr, R. E. Offeman, *Journal of the American Chemical Society*, 1958, **80**, 1339-.
34. L. Chen, S. Chai, K. Liu, N. Ning, J. Gao, Q. Liu, et al., *ACS applied materials & interfaces*, 2012, **4**, 4398-404.
35. J. L. Vickery, A. J. Patil, S. Mann, *Advanced Materials*, 2009, **21**, 2180-4.
36. T. H. Han, W. J. Lee, D. H. Lee, J. E. Kim, E. Y. Choi, S. O. Kim, *Advanced Materials*, 2010, **22**, 2060-4.
37. Y.-C. Chen, R. J. Young, J. V. Macpherson, N. R. Wilson, *The Journal of Physical Chemistry C*, 2007, **111**, 16167-73.
38. C. Xu, X. Wang, Small, 2009, 5, 2212-7.
39. A. Suspension. Characterization of chemically modified graphene sheets park. *Sungjin*.
40. W. Chen, L. Yan, P. R. Bangal, *Carbon*, 2010, **48**, 1146-52.
41. P. K. S. Mural, M. Sharma, G. Madras, S. Bose, *RSC Advances,* 2015, **5**, 32078-87.
42. J. Paredes, S. Villar-Rodil, P. Solis-Fernandez, A. Martinez-Alonso, J. Tascon, *Langmuir*, 2009, **25**, 5957-68.
43. V. C. Tung, M. J. Allen, Y. Yang, R. B. Kaner, *Nature nanotechnology*, 2009, **4**, 25-9.
44. S. Stankovich, D. A. Dikin, R. D. Piner, K. A. Kohlhaas, A. Kleinhammes, Y. Jia, et al., *Carbon*, 2007, **45**, 1558-65.
45. J. Liang, Y. Huang, L. Zhang, Y. Wang, Y. Ma, T. Guo, et al., *Advanced Functional Materials*, 2009, **19**, 2297-302.
46. X. Du, Z.-Z. Yu, A. Dasari, J. Ma, M. Mo, Y. Meng, et al., *Chemistry of Materials*, 2008, **20**, 2066-8.
47. M. Mahmoodi, M. Arjmand, U. Sundararaj, S. Park, *Carbon*, 2012, **50**, 1455-64.
48. A. K. Kota, B. H. Cipriano, M. K. Duesterberg, A. L. Gershon, D. Powell, S. R. Raghavan, et al., *Macromolecules*, 2007, **40**, 7400-6.
49. G. Sun, G. Chen, Z. Liu, M. Chen, *Carbon*, 2010, **48**, 1434-40.
50. H. Peng, X. Sun, *Chemical Physics Letters*, 2009, **471**, 103-5.
51. Y. Yang, M. Gupta, J. Zalameda, W. Winfree, *Micro & Nano Letters, IET*, 2008, **3**, 35-40.
52. H.-B. Zhang, W.-G. Zheng, Q. Yan, Z.-G. Jiang, Z.-Z. Yu, *Carbon*, 2012, **50**, 5117-25.
53. X.-Y. Qi, D. Yan, Z. Jiang, Y.-K. Cao, Z.-Z. Yu, F. Yavari, et al., *ACS applied materials & interfaces*, 2011, **3**, 3130-3.
54. W. Li, X.-Z. Tang, H.-B. Zhang, Z.-G. Jiang, Z.-Z. Yu, X.-S. Du, et al., *Carbon*, 2011, **49**, 4724-30.
55. D.-X. Yan, P.-G. Ren, H. Pang, Q. Fu, M.-B. Yang, Z.-M. Li, *Journal of Materials Chemistry*, 2012, **22**, 18772-4.
56. D. X. Yan, H. Pang, B. Li, R. Vajtai, L. Xu, P. G. Ren, et al., *Advanced Functional Materials*, 2015, **25**, 559-66.